

# Single Hyperspectral Image Super-resolution with Grouped Deep Recursive Residual Network

paper ID 151

**Abstract**—Fusing a low spatial resolution hyperspectral images (HSIs) with an high spatial resolution conventional (e.g., RGB) image has underpinned much of recent progress in HSIs super-resolution. However, such a scheme requires this pair of images to be well registered, which is often difficult to be complied with in real applications. To address this problem, we present a novel single HSI super-resolution method, termed Grouped Deep Recursive Residual Network (GDRRN), which learns to directly map an input low resolution HSI to a high resolution HSI with a specialized deep neural network. To well depict the complicated non-linear mapping function with a compact network, a grouped recursive module is embedded into the global residual structure to transform the input HSIs. In addition, we conjoin the traditional mean squared error (MSE) loss with the spectral angle mapper (SAM) loss together to learn the network parameters, which enables to reduce both the numerical error and spectral distortion in the super-resolution results, and ultimately improve the performance. Sufficient experiments on the benchmark HSI dataset demonstrate the effectiveness of the proposed method in terms of single HSI super-resolution. Pytorch implement of the proposed method will be available online.

**Index Terms**—Hyperspectral image (HSI), super-resolution (SR), deep network

## I. INTRODUCTION

Due to the advantages in conveying the spectral information of imaging scene, hyperspectral images (HSIs) have been extensively exploited in a wide spread of applications, such as remote sensing [1]–[3], biological recognition [4] and surveillance [5] etc. However, limited by physical sensors, raw hyperspectral images often exhibit low spatial resolution, which greatly impedes the wide applications of HSIs. Therefore, increasing HSIs super-resolution methods have been proposed to produce a high spatial resolution HSI given a low spatial resolution observation.

Most of existing HSIs super-resolution methods [6]–[8] focus on fusing a low spatial resolution HSI with a high spatial resolution conventional (e.g., RGB) image to produce a high spatial resolution HSI. Pingfan Song et al. [9] proposed a fusion based HSIs super-resolution method by learning coupled dictionary from pairs of low-resolution HSIs and corresponding high-resolution conventional images. Considering the non-local similarity, Weisheng Dong et al. [6] proposed Non-negative Structure Sparse Representation method to address this problem. Since the conventional image can provide abundant spatial information, these methods often can produce satisfactory super-resolution results. It is noteworthy that the success of these methods are underpinned by a basic assumption that the given HSI and the conventional image are

well registered. However, it is difficult to conform with such an assumption in practice.

To address this problem, an intutive solution is to directly improve the spatial resolution of the input low resolution HSI, which is often termed single HSI super-resolution. Currently, many single HSI super-resolution methods has been proposed. Most of early methods focus on improving the spatial resolution of an given observation with an appropriate interpolation strategy. For example, [10], [11]. However, due to not considering the inherent image characteristic, these interpolation methods cannot produce satisfactory super-resolution results. To this end, another line of research proposes to exploit the image statistical distribution as prior to cast the single HSI super-resolution into solving a regularized regression problem. For example, Yao Wang et al. [12] proposed an algorithm based on TV-regularization. Sparse representation [13] and self-similarity based methods [14] are also proposed to address this problem. Although these algorithms performed very well for conventional images, they ignored the correlation among spectral bands, which restrict the super-resolution effectiveness for HSIs. [13] proposed a more effective HSI SR model by exploiting the sparse property in both spectral and spatial domains. Although these methods obviously outperforms interpolation based ones, they still fails to appropriately recover the complex image details, since the expressive capacity of their shallow heuristic models is limited. Recently, deep neural network has been extensively investigated in various computer vision tasks. Due to the deep architecture, it is able to fit complicated non-linear mapping functions. For example, [15], [16].

Inspired by this, several literatures commenced at learning appropriate mapping functions for single HSI super-resolution. Yunsong Li et al. [17] learnt a deep mapping from spectral difference between neighbouring bands of low-resolution obser- vation to that of high-resolution, which achieved outstanding results compared with traditional algorithms. But their method need a large training set, about 95 hyperspectral images from three publicly available datasets. Shaohui Mei et al. [18] proposed 3D Full-CNN model to address this problem. Although 3D convolution may preserve more information of spectral correlation, the computational complexity is very large. Sen Lei et al. [19] try to learn multi-level representation by Local- Global Combined Network. While effective, these methods contain too many parameters, which require extensive training examples for training. Moreover, it impedes the network going deeper for better generalization capacity.

In this study, we present a novel single HSI super-resolution

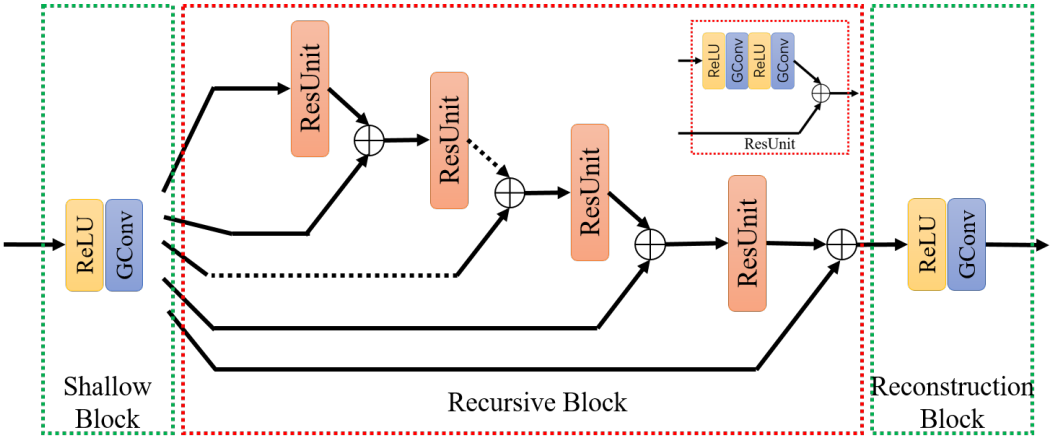


Fig. 1. Structure of proposed Grouped Deep Recursive Residual network, where 'GConv' denotes group-wise convolution.

method, termed Grouped Deep Recursive Residual Network (GDRRN). In this network, we develop a new grouped recursive module and embed into the global residual structure to map the input low resolution HSI into a high resolution HSI. By doing this, the complicated no-linear mapping function for single HSI super-resolution can be well depicted. Moreover, both the group-wise convolution and recursive structure can greatly reduce the network parameters to enable a deeper model. In addition, we conjoin the traditional mean squared error (MSE) loss with the spectral angle mapper (SAM) loss together to learn the network parameters, which enables to reduce both the numerical error and spectral distortion in the super-resolution results. With sufficient experiments on the benchmark HSI dataset, the proposed method shows pleasing potential in terms of single HSI super-resolution.

The paper is organized as follows. Section II describes proposed GDRRN method for HSI super-resolution. Experimental results are shown in Section III. Finally, we will give a conclusion in Section IV.

## II. GROUPED DEEP RECURSIVE RESIDUAL NETWORK

The proposed structure of GDRRN is shown in Fig. 1. Given a single low-resolution HSI  $\mathbf{X} \in \mathbb{R}^{L \times w \times h}$ , we want to learn a mapping from  $\mathbf{X}$  to ideal high resolution HSI  $\mathbf{Y} \in \mathbb{R}^{L \times W \times H}$ .  $w, h, L$  denote the width, height, and spectral bands of low-resolution HSI and  $W, H$  is the width, height of high-resolution HSI. In this section, we firstly detail DRRN structure applied in proposed method, and then group-wise version. Finally we introduce a new training loss to preserve spectral profiles of reconstructed HSIs.

### A. Deep Recursive Residual Network

In [15], deep recursive residual network (DRRN) is proposed to provide a compact network which contains much less parameters than that in traditional fully convolutional networks. As shown in Fig. 1, DRRN consists of three parts, including the shallow feature block, recursive residual block and the reconstruction block. Specifically, suppose  $X$  and  $H^0$

as the input and output of Shallow Block, the mapping function can be formulated as,

$$H^0 = \mathcal{S}(X) = Conv(ReLU(X)) \quad (1)$$

where  $\mathcal{S}(\bullet)$  represent the mapping function of Shallow Block. Providing that  $H^{u-1}$  and  $H^u$  denote  $(u-1)$ th and  $u$ th residual units respectively, the  $u$ th residual unit can be defined as follows,

$$H^u = \mathcal{G}_u(H^{u-1}) = \mathcal{F}(H^{u-1}; \theta_u) + H^0 \quad (2)$$

where  $\theta_u$  denotes parameters of the  $u$ th residual unit. To reduce the parameters, all residual units shared the same weights, i.e. recursively using the same single residual unit. At the end, the result of recursive block is defined as follows,

$$\begin{aligned} H^1 &= \mathcal{G}^{(1)}(H^0) = \mathcal{G}(H^0) \\ H^2 &= \mathcal{G}^{(2)}(H^0) = \mathcal{G}(\mathcal{G}(H^0)) \\ &\dots \\ H^U &= \mathcal{G}^{(U)}(H^0) = \underbrace{\mathcal{G}(\mathcal{G}(\dots \mathcal{G}(H^0)))}_U \end{aligned} \quad (3)$$

where  $U$  is the number of recursion. Finally, feature maps from Recursive Block are fed into Reconstruction Block to generate reconstructed images. In proposed method, we set  $U = 9$ . More details about DRRN can be found in authors' paper [15].

### B. Group-wise Convolution

Group-wise convolution was proposed to reduce number of parameters of networks. As shown in Fig. 2, group-wise convolution separate input feature maps into  $N$  groups, and each of them corresponds to independent convolution. Using this schema, the number of parameters can be reduced by  $N$  times.

Xiangyu Zhang et al. introduced group-wise convolution to ShuffleNet to handle the issue of network compression [20]. In this paper, we replace original convolutional layers with group-wise convolution to reduce more parameters.

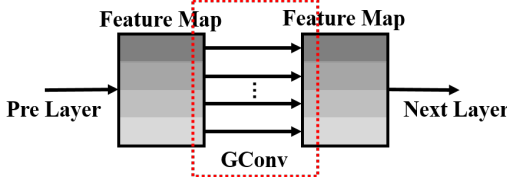


Fig. 2. Group-wise convolution.

### C. Joint Loss (JL)

For deep learning based image super-resolution methods, mean squared error (MSE) is often adopted for training the network. Let  $\mathcal{H}(\bullet; \theta)$  represent a pre-trained network and  $Y = \mathcal{H}(X; \theta)$  denote the output of this network given an input  $X$ , then the formulation of MSE loss can be given as,

$$MSE(Y, Z) = \frac{1}{N_m} \sum_j \|\hat{\mathbf{y}}_j - \mathbf{z}_j\|_2^2 \quad (4)$$

where  $\hat{\mathbf{y}}_j$  and  $\mathbf{z}_j$  denote  $j$ th pixel from the estimated image and ground truth  $Z$ , respectively.  $N_m$  is total number of pixels on this HSI. It is noticeable that strong correlation often exists among spectral bands of a given HSI. However, the MSE loss considers each band independently and thus fails to preserve the correlation among different bands.

To address this problem, we develop a new loss based on the spectral angle mapper (SAM) [21] criterion for HSI quality assessment. The definition of SAM-Loss can be formulated as

$$SAM(Y, Z) = \frac{1}{N_m} \sum_j \arccos \frac{\hat{\mathbf{y}}_j^\top \mathbf{z}_j}{\|\hat{\mathbf{y}}_j\|_2 \|\mathbf{z}_j\|_2} \quad (5)$$

It can be found that SAM-loss considers each spectrum as a whole and measures the angle between the reconstructed spectrum and the reference. Thus, minimizing the SAM-loss is able to encourage the network to preserve the spectral profile of the output.

To reduce both the numerical error and the spectral distortion in the super-resolution results, we conjoin MSE loss with SAM loss together to train the network as,

$$L(\mathcal{H}(X; \theta), Z) = MSE(\mathcal{H}(X; \theta), Z) + \lambda SAM(\mathcal{H}(X; \theta), Z) \quad (6)$$

where  $\lambda$  is a pre-defined balance factor (e.g.,  $0 \leq \lambda \leq 1$ ).

## III. EXPERIMENTAL RESULTS

In this section, we conduct sufficient experiments to demonstrate the effectiveness of the proposed method in terms of single HSI super-resolution.

### A. Datasets

In this study, we adopt the Harvard dataset [22] as benchmark, which contains 50 indoor and outdoor HSIs with 31 spectral bands ranging from 420nm to 720nm. The spatial resolution of each image is  $1024 \times 1024$ . For the training dataset, we randomly choose five hyperspectral images ("img1", "imgb3", "imgc5", "imge0", "imgf3") and crop

$32 \times 32$  patches with a stride of 16 in each image. To generate the low-resolution observations, we down-sample each extracted patch with scaling factor 2, 4 and 8, respectively. In addition, we augment the training data with rotation (e.g., with angle  $90^\circ, 180^\circ, 270^\circ$ ), flipping up and scaling (e.g., with factor 1, 0.5, 0.25). Finally, we obtain 206,208 patches for every scaling factor. The rest of images in Harvard dataset are regarded as test dataset. For testing efficiency, we crop top-left  $512 \times 512$  pixels in each test image for evaluation.

### B. Implementation Details

In the training phase, we empirically choose a mini-batch size of 32, and use Adam optimizer with weight decay of 1e-4. We train proposed network using 30 epochs. The initial learning rate is set as 0.0001 and is decayed by 10 times after 20 epochs. The balance factor  $\lambda$  between MSE loss and SAM-Loss is set to be  $\lambda = 0.1$ . The proposed method is evaluated on an NVIDIA GeForce GTX1080Ti with 11GB memory, and training the proposed network takes about 2.5 hours on average.

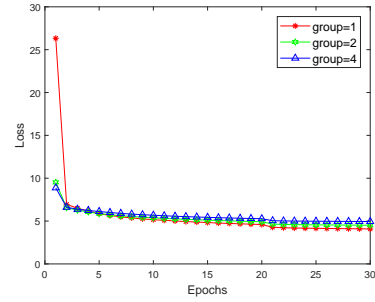


Fig. 3. Training loss from the proposed method with different group numbers in group-wise convolution.

TABLE I

PERFORMANCE OF THE PROPOSED METHOD WITH DIFFERENT GROUP NUMBERS IN GROUP-WISE CONVOLUTION ON HARVARD DATASET WITH A SCALING FACTOR 4. (THE BEST RESULTS ARE IN **BOLD**, AND THE SECOND BEST ARE UNDERLINED.)

	Bicubic	GDRRN-g1	GDRRN-g2	GDRRN-g4
PSNR	35.075	36.568	<b>36.736</b>	36.657
SAM	<b>2.689</b>	<u>2.702</u>	2.724	2.722
UIQI	0.953	<u>0.964</u>	<b>0.965</b>	0.964
ERGAS	0.509	<u>0.441</u>	<b>0.438</b>	0.444
Parameters	-	366K	219K	145K

### C. Evaluation Indices

To quantitatively measure the proposed method, we choose four prevailing evaluation indices, including Peak Signal Noise Rate (PSNR), Spectral Angle Mapper (SAM), Universal Image Quality Index (UIQI) [23] and *Erreur Relative Globale Adimensionnelle de Synthèse* (ERGAS) [24].

### D. Effect of the group-wise convolution

To evaluate the effectiveness of group-wise convolution, we train proposed network with group number 1, 2 and 4. The

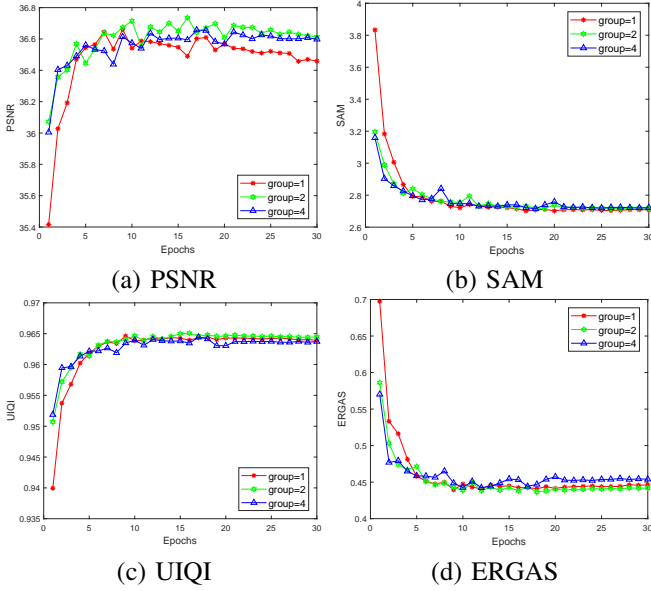


Fig. 4. The performance curves of the proposed method with different group numbers in group-wise convolution on Harvard dataset with a scaling factor 4 in 30 epochs.

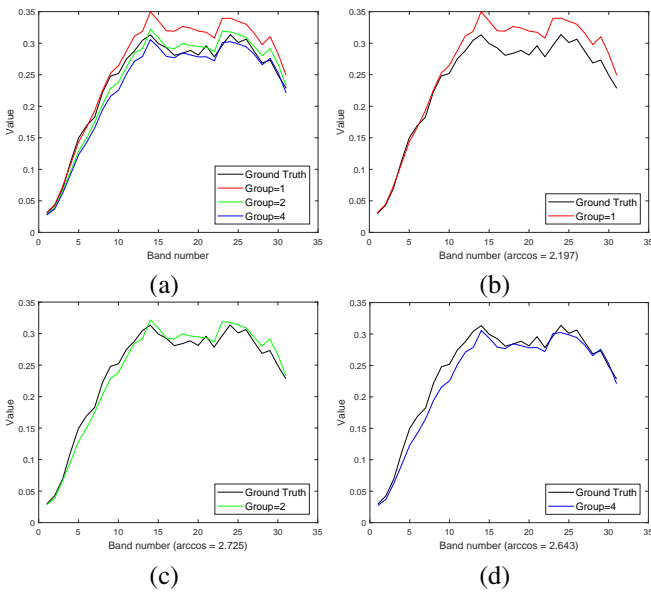


Fig. 5. Spectral profiles of the proposed method with different group numbers in group-wise convolution on Harvard dataset with a scaling factor 4.

corresponding training loss curves are depicted in Fig. 3. From these loss curve, we find that large group number leads to fast convergence to a slightly high final loss. The corresponding PSNR, SAM, UIQI and ERGAS numerical results and curves on test dataset are reported in Fig. 4 and Table I. The spectral curves from the reconstructed 'img2' images are shown in Fig. 5. It can be found that the proposed method achieves the best results on PSNR, UIQI and ERGAS when group number is 2.

TABLE II  
COMPARISONS BETWEEN MSE LOSS AND SAM LOSS ON HARVARD DATASET WITH A UPSCALE FACTOR OF 4 AND THE GROUP NUMBER IS 2.  
(THE BEST RESULTS ARE IN BOLD, AND THE SECOND BEST ARE UNDERLINED.)

	GDRRN-MSE	GDRRN-SAM	GDRRN-JL
PSNR	<b>36.736</b>	35.180	<u>36.728</u>
SAM	2.724	<b>2.629</b>	2.708
UIQI	<b>0.965</b>	0.955	<b>0.965</b>
ERGAS	0.438	0.491	<b>0.437</b>

#### E. Effect of the joint loss

In this study, we introduce the SAM loss to preserve spectral correlation among different bands in the super-resolution results. To demonstrate this point, we implement two variants of the proposed method with training the same network with MSE loss and SAM loss separately. The performance curves and numerical results of these three methods are provided in Fig. 6 and Table. II. Comparison of spectral curves from reconstructed 'img2' images are shown in Fig. 7. From Fig. 6, we find that the proposed method training using SAM loss achieves much lower value on SAM measurement compared with MSE loss, but its performance on other measurements degrades quickly after 5th epoch. Similar results can be found on Fig. 7. Although the shape of the spectral band reconstructed using SAM loss is more similar to ground truth, MSE loss leads to more closer spectral profile. The reason may be that SAM loss directly optimizes SAM value of reconstructed images, but the overall amplification of a pixel's value could lead to the same value of SAM measurement and degrade other measurements. Joint loss function (SAM+MSE) could make up spectral distortion of reconstructed images using MSE loss. For example, the 20th band of this pixel reconstructed using joint loss is closer to ground truth compared with which reconstructed using MSE loss. These results indicate the effectiveness of the proposed joint loss function (JL).

#### F. Comparison with other methods

We compare proposed method with several methods include Bicubic, Bilinear, DRRN without group-wise convolution and 4-layers CNN (SRConv4) implemented by ourselves whose parameter number is as same as DRRN.

Final reconstructed results of proposed method on Harvard dataset are shown in Fig. 8, Fig. 9 and Table. III. Fig. 8 shows visualized results of 31th spectral band and absolute error maps of 'imga1' reconstructed by different methods with a upscale factor of 2. As shown, Bicubic and Bilinear perform worse than other deep learning based methods, especially on edge textures. Compared with SRConv4 and DRRN, proposed method preserves more details. For example, on the edges of top-left window, the error map of proposed method is darker than competing methods. Similar results can be found in Fig. 9, which gives visualized results of 31th spectral band and absolute error maps of 'imgb9' with a upscale factor of 4. To evaluate spectral preservation capability of proposed method, we extract one pixel from corresponding reconstructed images

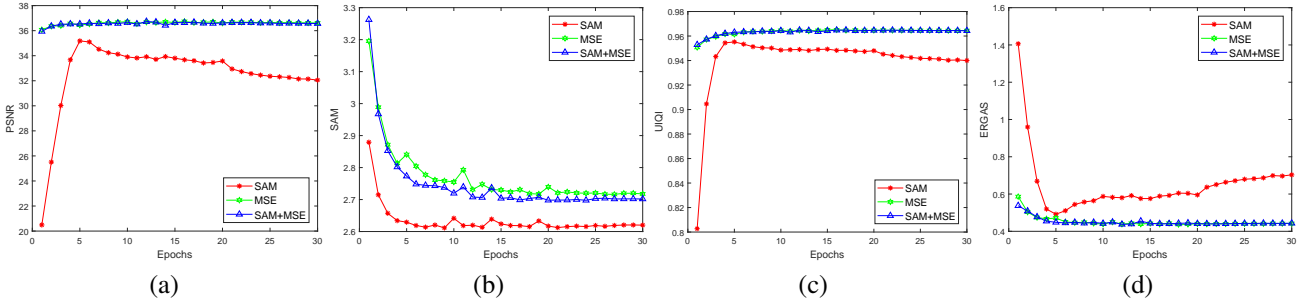


Fig. 6. (a), (b), (c), (d) are PSNR, SAM, UIQI, ERGAS comparisons between MSE Loss and SAM Loss on Harvard dataset, respectively, with a upscale factor of 4 and the group number is 2.

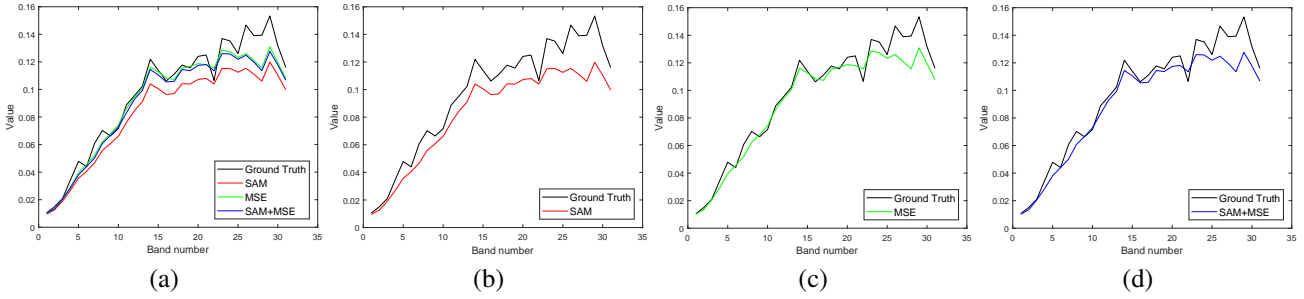


Fig. 7. Spectral profile comparison on Harvard dataset with different loss functions.

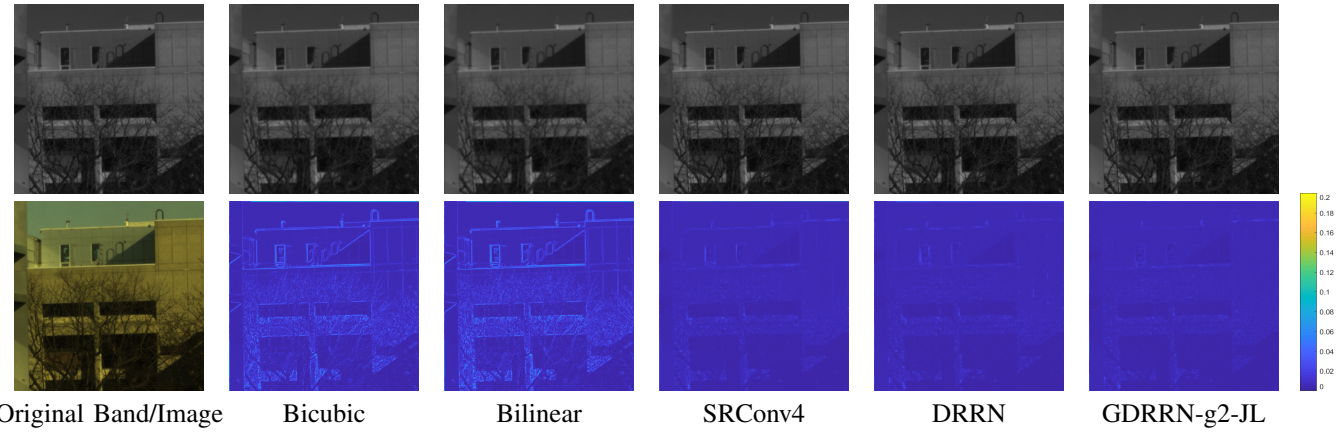


Fig. 8. Reconstruction results and error maps of 'imga1' image from Harvard dataset with a upscale factor of 2. First row includes original/reconstructed images on the 31th band. Second row shows the error maps with color bar.

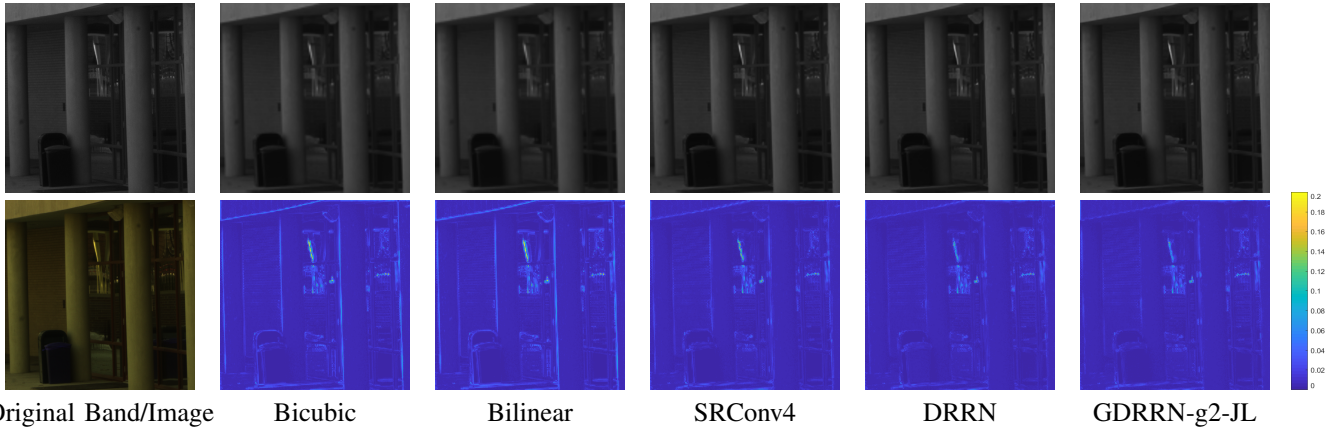


Fig. 9. Reconstruction results and error maps of 'imgb9' image from Harvard dataset with a upscale factor of 4. First row includes original/reconstructed images on the 31th band. Second row shows the error maps with color bar.

TABLE III

EXPERIMENTAL RESULTS COMPARISON ON HARVARD DATASET. (THE BEST RESULTS ARE IN BOLD, AND THE SECOND BEST ARE UNDERLINED.)

Parameters	Bicubic	Bilinear	SRConv4	DRRN	GDRRN-g2-JL
	-	-	366K	366K	219K
	$\times 2$				
PSNR	37.413	36.992	41.836	<u>42.163</u>	<b>42.445</b>
SAM	2.327	2.391	2.196	2.226	<b>2.175</b>
UIQI	0.973	0.970	<b>0.988</b>	<b>0.988</b>	<b>0.988</b>
ERGAS	0.390	0.410	0.255	0.254	<b>0.244</b>
	$\times 4$				
PSNR	35.075	34.509	36.305	36.644	<b>36.728</b>
SAM	<b>2.689</b>	2.739	<u>2.708</u>	2.762	<u>2.708</u>
UIQI	0.953	0.947	0.963	0.964	<b>0.965</b>
ERGAS	0.509	0.540	0.457	0.447	<u>0.437</u>
	$\times 8$				
PSNR	32.059	31.658	32.482	32.552	<b>32.671</b>
SAM	<b>3.062</b>	<u>3.102</u>	3.148	3.219	3.113
UIQI	0.912	0.904	0.919	<u>0.920</u>	<b>0.921</b>
ERGAS	0.706	0.737	0.681	0.678	<b>0.664</b>

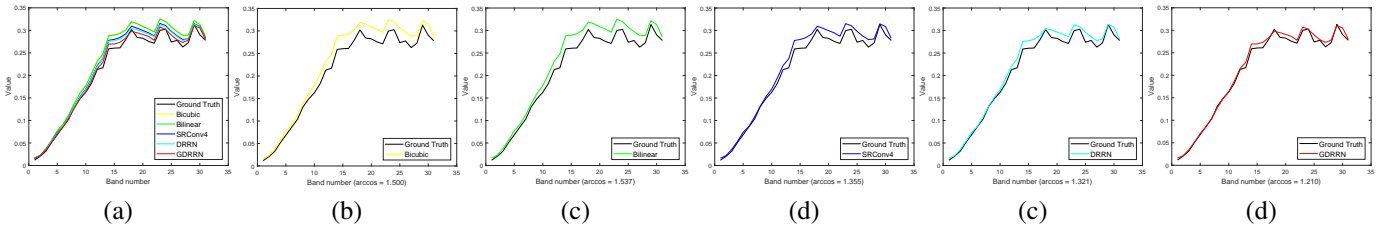


Fig. 10. Spectral profile comparisons on Harvard dataset with a upscale factor of 2.

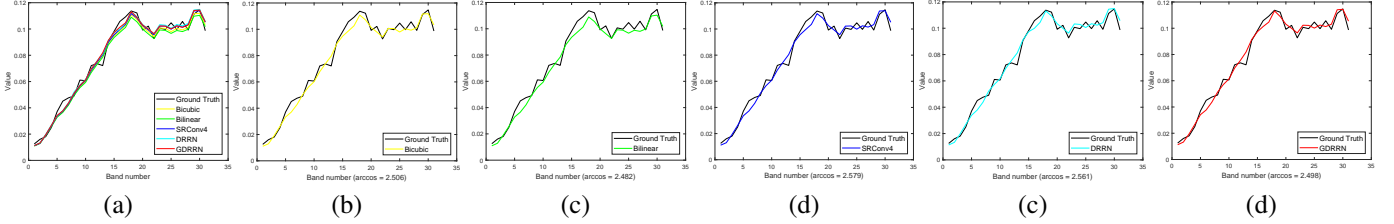


Fig. 11. Spectral profile comparisons on Harvard dataset with a upscale factor of 4.

and plot spectral profiles in Fig. 10 and Fig. 11. Values of arc cosine between ground truth and reconstructed spectral are list under each figure. From these results, we find that Bicubic and Bilinear method can preserve spectral files of HSIs very well compared with proposed method when upscale factor is large.

#### IV. CONCLUSION

In this study, we present a Grouped Deep Recursive Residual Network (GDRRN) for single HSI super-resolution. Through introducing the recursive residual block into a global residual block, the non-linear mapping between the low resolution HSI and the high resolution image can be well depict. Moreover, both the group-wise convolution and the recursive structure enable the network to be compact. In addition, we develop a joint loss for training network, which conjoins the traditional MSE loss with the SAM based loss and thus can reduce the numerical error as well as the spectral distortion in the obtained super-resolution result. Sufficient experimental results on publicly available dataset demonstrate that the

promising potential of the proposed method in terms of single HSI super-resolution.

#### REFERENCES

- [1] Jose M Bioucasdias, Antonio Plaza, Gustavo Campsvals, Paul Scheunders, Nasser M Nasrabadi, and Jocelyn Chanussot, "Hyperspectral remote sensing data analysis and future challenges," *IEEE Geoscience and Remote Sensing Magazine*, vol. 1, no. 2, pp. 6–36, 2013.
- [2] Lei Zhang, Wei Wei, Yanning Zhang, Chunhua Shen, Anton van den Hengel, and Qinfeng Shi, "Cluster sparsity field for hyperspectral imagery denoising," in *European Conference on Computer Vision*. Springer, 2016, pp. 631–647.
- [3] Cong Wang, Lei Zhang, Wei Wei, and Yanning Zhang, "When low rank representation based hyperspectral imagery classification meets segmented stacked denoising auto-encoder based spatial-spectral feature," *Remote Sensing*, vol. 10, no. 2, pp. 284, 2018.
- [4] Muhammad Uzair, Arif Mahmood, and Ajmal S Mian, "Hyperspectral face recognition using 3d-dct and partial least squares," in *BMVC*, 2013.
- [5] Fernando Vanegas, Dmitry Bratanov, Kevin Powell, John Weiss, and Felipe Gonzalez, "A novel methodology for improving plant pest surveillance in vineyards and crops using uav-based hyperspectral and spatial data," *Sensors*, vol. 18, no. 1, pp. 260, 2018.
- [6] Weisheng Dong, Fazuo Fu, Guangming Shi, Xun Cao, Jinjian Wu, Guangyu Li, and Xin Li, "Hyperspectral image super-resolution via

- non-negative structured sparse representation.” *IEEE Transactions on Image Processing*, vol. 25, no. 5, pp. 2337–2352, 2016.
- [7] Charis Lanaras, Emmanuel Baltasvias, and Konrad Schindler, “Hyperspectral super-resolution by coupled spectral unmixing,” in *Proceedings of the IEEE International Conference on Computer Vision*, 2015, pp. 3586–3594.
- [8] Yong Li, Lei Zhang, Chunna Tian, Chen Ding, Yanning Zhang, and Wei Wei, “Hyperspectral image super-resolution extending: An effective fusion based method without knowing the spatial transformation matrix,” in *Multimedia and Expo (ICME), 2017 IEEE International Conference on*. IEEE, 2017, pp. 1117–1122.
- [9] Pingfan Song, Xin Deng, João FC Mota, Nikos Deligiannis, Pier Luigi Dragotti, and Miguel RD Rodrigues, “Multimodal image super-resolution via joint sparse representations induced by coupled dictionaries,” *arXiv preprint arXiv:1709.08680*, 2017.
- [10] Wan-Chi Siu and Kwok-Wai Hung, “Review of image interpolation and super-resolution,” in *Signal & Information Processing Association Annual Summit and Conference (APSIPA ASC), 2012 Asia-Pacific*. IEEE, 2012, pp. 1–10.
- [11] Xin Li and Michael T Orchard, “New edge-directed interpolation,” *IEEE transactions on image processing*, vol. 10, no. 10, pp. 1521–1527, 2001.
- [12] Yao Wang, Xiai Chen, Zhi Han, Shiying He, et al., “Hyperspectral image super-resolution via nonlocal low-rank tensor approximation and total variation regularization,” *Remote Sensing*, vol. 9, no. 12, pp. 1286, 2017.
- [13] Jie Li, Qiangqiang Yuan, Huanfeng Shen, Xiangchao Meng, and Liangpei Zhang, “Hyperspectral image super-resolution by spectral mixture analysis and spatial-spectral group sparsity,” *IEEE Geoscience and Remote Sensing Letters*, vol. 13, no. 9, pp. 1250–1254, 2016.
- [14] Zongxu Pan, Jing Yu, Huijuan Huang, Shaoxing Hu, Aiwu Zhang, Hongbing Ma, and Weidong Sun, “Super-resolution based on compressive sensing and structural self-similarity for remote sensing images,” *IEEE Transactions on Geoscience and Remote Sensing*, vol. 51, no. 9, pp. 4864–4876, 2013.
- [15] Ying Tai, Jian Yang, and Xiaoming Liu, “Image super-resolution via deep recursive residual network,” in *The IEEE Conference on Computer Vision and Pattern Recognition (CVPR)*, 2017, vol. 1.
- [16] Bee Lim, Sanghyun Son, Heewon Kim, Seungjun Nah, and Kyoung Mu Lee, “Enhanced deep residual networks for single image super-resolution,” in *The IEEE Conference on Computer Vision and Pattern Recognition (CVPR) Workshops*, 2017, vol. 1, p. 3.
- [17] Yunsong Li, Jing Hu, Xi Zhao, Weiyang Xie, and JiaoJiao Li, “Hyperspectral image super-resolution using deep convolutional neural network,” *Neurocomputing*, vol. 266, pp. 29–41, 2017.
- [18] Shaohui Mei, Xin Yuan, Jingyu Ji, Yifan Zhang, Shuai Wan, and Qian Du, “Hyperspectral image spatial super-resolution via 3d full convolutional neural network,” *Remote Sensing*, vol. 9, no. 11, pp. 1139, 2017.
- [19] Sen Lei, Zhenwei Shi, and Zhengxia Zou, “Super-resolution for remote sensing images via local-global combined network,” *IEEE Geoscience and Remote Sensing Letters*, vol. 14, no. 8, pp. 1243–1247, 2017.
- [20] Xiangyu Zhang, Xinyu Zhou, Mengxiao Lin, and Jian Sun, “Shufflenet: An extremely efficient convolutional neural network for mobile devices,” *arXiv preprint arXiv:1707.01083*, 2017.
- [21] Roberta H Yuhas, Alexander FH Goetz, and Joe W Boardman, “Discrimination among semi-arid landscape endmembers using the spectral angle mapper (sam) algorithm,” 1992.
- [22] Ayan Chakrabarti and Todd Zickler, “Statistics of real-world hyperspectral images,” in *Computer Vision and Pattern Recognition (CVPR), 2011 IEEE Conference on*. IEEE, 2011, pp. 193–200.
- [23] Zhou Wang and Bovik Alan C, “A universal image quality index,” *IEEE Signal Processing Letters*, vol. 9, no. 3, pp. 81–84, 2002.
- [24] Lucien Wald, “Quality of high resolution synthesised images: Is there a simple criterion?”, in *Third conference “Fusion of Earth data: merging point measurements, raster maps and remotely sensed images”*. SEE/URISCA, 2000, pp. 99–103.